

Supplementary material

Triple-functional Co_2SnO_4 -enabled S-scheme heterojunction with photothermal promotion for efficient solar-driven hydrogen evolution

Kai Li^{a,†}, Zhaochao Yan^{a,†}, Shuhan Sun^a, Qianmin Fan^a, Huayue Zhu^b, Chenglin Wu^{a,*}, Yanxian Jin^a,

Sónia A.C. Carabineiro^{c,*}, Ruiqiang Yan^a, Bingjing He^a, Xianqiang Xiong^{a,*}

^a*Zhejiang Key Laboratory for Island Green Energy and New Materials, Taizhou University, Taizhou, 318000, P.R. China*

^b*Institute of Environmental Engineering Technology, Taizhou University, Taizhou, 318000, Zhejiang, P. R. China*

^c*LAQV-REQUIMTE, Department of Chemistry, NOVA School of Science and Technology, Universidade NOVA de Lisboa, Caparica 2829-516, Portugal*

**Corresponding author: polyclwu@126.com (C. L. Wu), sonia.carabineiro@fct.unl.pt (S.A.C. Carabineiro), 11337061@zju.edu.cn (X. Q. Xiong)*

†These authors contributed equally to this work.

1. Experimental Details

1.1 Materials

Zinc chloride (ZnCl_2 , $\geq 98.0\%$), Indium (III) trichloride ($\text{InCl}_3 \cdot 4\text{H}_2\text{O}$, 99.99%), Thioacetamide (TAA) ($\geq 98.0\%$), $\text{Na}_2\text{S}_2\text{O}_3 \cdot 6\text{H}_2\text{O}$ (99%), $\text{Co}(\text{NO}_3)_2 \cdot 6\text{H}_2\text{O}$ (99.99%), SnCl_4 ($\geq 98.0\%$), Triethanolamine (TEOA), $\text{Na}_2\text{S} \cdot 9\text{H}_2\text{O}$ ($\geq 98.0\%$), Na_2SO_3 (98.0%) Ascorbic acid (AA, $\geq 99\%$) and Na_2SO_4 ($\geq 99\%$) were all purchased from Aladdin. Methanol (MeOH, 99.99%) and Ethylene glycol (EG) were purchased from Honeywell. Lactic acid (85%~90%) was purchased from Macklin. $\text{HAuCl}_4 \cdot 3\text{H}_2\text{O}$ ($\geq 99.9\%$) and H_2PtCl_6 (8 wt% in H_2O) were obtained from Sigma-Aldrich. Ethanol was purchased from Sinopharm Chemical Reagent Co., Ltd. Fluorine-doped tin oxide glass (FTO) was sourced from Nippon Sheet Glass Co. Ltd, and cleaned by sonication in ultrapure water, ethanol and acetone for 15 minutes, followed by drying under N_2 at room temperature. Deionized (DI) water was used for the preparation of the reaction solutions.

1.2 Preparation of Co_2SnO_4 nanoparticles

The synthesis of Co_2SnO_4 was carried out as follows: Initially, 4 mmol of $\text{Co}(\text{NO}_3)_2 \cdot 6\text{H}_2\text{O}$ was dissolved in 30 mL of deionized water with continuous stirring at room temperature until a homogeneous solution, referred to as Solution A, was obtained. Simultaneously, 2 mmol of $\text{SnCl}_4 \cdot 5\text{H}_2\text{O}$ was dissolved in 20 mL of deionized water under the same conditions to form Solution B. Solution A was then added to Solution B, and the mixture was stirred for an additional 10 minutes at room temperature to produce Solution C. Following this, 20 mL of a 1 mol/L NaOH solution was added to Solution C, and the mixture was stirred for 30 minutes, resulting in the formation of a blue precipitate. This mixture was then transferred into a 100 mL Teflon-lined stainless-steel autoclave and heated at 180 °C for 10 h. After cooling to room temperature, the mixture was filtered, and the resulting

CoSn(OH)₆ was sequentially washed with deionized water and ethanol, followed by drying in an oven at 60 °C. Finally, 100 mg of CoSn(OH)₆ was placed in a crucible and calcined at 500 °C for 3 h in a muffle furnace, yielding Co₂SnO₄ nanoparticles.

1.3 Preparation of ZnIn₂S₄ nanosheets

ZnIn₂S₄ nanosheets were synthesized using a simple low-temperature oil bath technique, as described in previous literature. In a typical synthesis¹, 136.3 mg of ZnCl₂ and 586.5 mg of InCl₃·4H₂O were dissolved in 100 mL of deionized water. Subsequently, 450.5 mg of thioacetamide (TAA) was added into the solution and the mixture was stirred for 10 min until fully dissolved. The resulting solution was then continuously stirred in an oil bath maintained at 80 °C for 6 h. After the reaction, the system was allowed to cool to room temperature. The resulting ZnIn₂S₄ powders were collected by filtration, followed by thorough washing with water and ethanol. Finally, the powders were dried at 60 °C in an oven.

1.4 Preparation of x %-Co₂SnO₄@ZnIn₂S₄

The Co₂SnO₄@ZnIn₂S₄ composite was synthesized through a simple solvent self-assembly process involving Co₂SnO₄ nanoparticles and ZnIn₂S₄ nanosheets. In a typical experiment², 50 mg of ZnIn₂S₄ nanosheets was dispersed in 30 mL of deionized water. A predetermined amount of Co₂SnO₄ nanoparticles was then added to the ZnIn₂S₄ suspension. The mixture was stirred for 2 h at room temperature, after which the precipitate was collected by filtration and washed thoroughly with deionized water. By varying the amount of Co₂SnO₄ nanoparticles added to the suspension (5%, 10%, 20% and 30%), Co₂SnO₄@ZnIn₂S₄ composites with different Co₂SnO₄ nanoparticle contents were

synthesized. These composites were designated as 5%-Co₂SnO₄@ZnIn₂S₄, 10%-Co₂SnO₄@ZnIn₂S₄, 20%-Co₂SnO₄@ZnIn₂S₄ and 30%-Co₂SnO₄@ZnIn₂S₄, respectively.

1.5 Preparation of Pt@ZIS and Au@ZIS

Pt@ZIS: Typically, 500 mg of monoclinic ZnIn₂S₄ was dispersed into 100 mL deionized water containing 0.5 wt% H₂PtCl₆ as the hole scavenger. The resulting suspension was stirred for 30 min in a dark environment to ensure complete mixing. The mixture was then subjected to visible light illumination for 2 h. During the photoreduction process, H₂PtCl₆ was reduced, leading to the formation of Pt nanoparticles, which were subsequently deposited on the surface of ZnIn₂S₄. After the photoreduction reaction, the resulting powders were washed thoroughly, collected and then dried at 80 °C.

Au@ZIS: 100 mg of ZnIn₂S₄ was dispersed into 100 ml of deionized water to obtain a homogeneous suspension. Then 0.5 wt% HAuCl₄ was added to the suspension and stirred for 30 min. Before photo-irradiation, the suspension was purged with pure N₂ for 30 mins. The mixture was then illuminated under visible light for 3 h. After the photoreduction reaction, the obtained powders were filtered, washed thoroughly with deionized water, and dried at 80 °C for 12 h.

1.6 Characterizations

A series of characterizations was conducted on the prepared samples. Powder X-ray diffraction (PXRD) diffractograms were collected using a Bruker D8 diffractometer to analyze the crystal structures of the samples. The optical absorption properties of Co₂SnO₄, ZnIn₂S₄ and *x* %-Co₂SnO₄@ZnIn₂S₄ samples were examined using an ultraviolet-visible (UV-vis) diffuse reflectance spectroscopy (DRS) using a Hitachi U-4100 spectrophotometer (Japan). To observe the surface

morphologies, scanning electron microscopy (SEM) images were obtained using a Hitachi S-4800 field-emission scanning electron microscope (FESEM), while high-resolution transmission electron microscopy (HRTEM) images were collected using a JEM-2100F high-resolution transmission electron microscope. The surface chemistry of the samples was analyzed using X-ray photoelectron spectroscopy (XPS and UPS) with a Thermo Fisher Scientific Escalab 250Xi X-ray photoelectron spectrometer, equipped with an Al-K α source (150 W), and the data were processed with Thermo Avantage 5.9931 software for curve fitting. The Brunauer-Emmett-Teller (BET) surface areas and pore structures of the samples were determined using N₂ adsorption and desorption analysis on a Micromeritics ASAP 2020 apparatus (USA) at -196°C. The steady-state and time-resolved photoluminescence (PL) spectra were recorded on a Horiba Hobin Yvon HUB fluorescence spectrophotometer, using excitation and emission wavelengths of 250 nm and 300 nm, respectively. Surface photovoltage spectroscopy (SPS) measurements were performed using a lock-in-based SPS apparatus that includes a lock-in amplifier (SR830-DSP), a light chopper (SR540), a photovoltaic cell and a computer for signal processing. The surface potential distributions were measured using Kelvin probe force microscopy (KPFM) with an AIST-NT atomic force microscope. The Zeta potentials were measured using a Zetasizer Nano ZS90.

1.7 Photoelectrochemical and impedance measurements

The photoanode for photocatalytic testing was prepared using a solution coating method. To begin, 20 mg of the powder sample was dispersed in 2 mL of ethanol, along with 200 μ L of Nafion solution, and subjected to ultrasonic treatment for 50 min. Afterwards, 100 μ L of the resulting suspension was spread onto a FTO substrate, which was then dried at 60 °C to form the photoanode. To conduct the

test, a saturated Ag/AgCl electrode was used as the reference electrode, a platinum foil served as the counter electrode, and the photoanode was functioned as the working electrode, which was illuminated with a 300 W Xenon lamp. Electrochemical impedance spectroscopy (EIS) was performed using a CHI760E Electrochemical Station (Chenhua, Shanghai) over a frequency range of 10 mHz–100 kHz with an amplitude of 10 mV. The impedance data were fitted with Z-view software by selecting an appropriate equivalent circuit.

1.8 Hydrogen evolution reaction (HER) activity test

The photocatalytic H₂ evolution reaction was performed in a glass gas close-circulation system (CEL-PAEM-D8Plus), purchased from Beijing China Education Au-light Co., Ltd. In a typical hydrogen production experiment, 25 mg of the as-synthesized photocatalyst was dispersed in a mixed aqueous solution containing 10 mL triethanolamine (TEOA, sacrificial agent) and 40 mL of deionized water. The resulting solution was continuously stirred to maintain the photocatalyst in suspension, while a cooling water circulation system was employed to keep the reaction temperature at 6°C. Before the start of the experiment, the solution was degassed for 30 min using a vacuum pump to remove dissolved air. The aqueous suspension was then irradiated from the top using a 300 W Xenon lamp (CEL-HXF 300-T3). The generated H₂ gas was monitored in real-time using gas chromatography (GC-7920-TF2A) equipped with a TCD detector.

To assess the stability and reusability for long-time illumination in practical applications, a recycling test was conducted using the optimal 20 %-Co₂SnO₄@ZnIn₂S₄ composite under the same experimental conditions. After 2 h of Xenon light illumination, the photocatalytic H₂ generation system was

vacuumed to remove the generated H₂. The cyclical test of the optimal 20 %-Co₂SnO₄@ZnIn₂S₄ composite was performed continuously for 5 cycles under the same test conditions.

The apparent quantum efficiency (AQE) experiment was conducted under similar conditions with 4 h of illumination. The AQE for H₂ production was calculated using the following equation³:

$$AQE = \frac{2n(H_2) \times N_0(mol^{-1})}{\frac{t(s) \times P(W \cdot cm^{-2}) \times S(cm^2) \times \lambda(m)}{h(J \cdot s) \times c(m \cdot s^{-1})}} \times 100\%$$

Where $n(H_2)$ is the molar amount of H₂ production (0.13 mmol·g⁻¹, 25 mg of catalyst), N_0 is Avogadro's constant (6.022×10²³ mol⁻¹), $t(s)$ is the illumination time (4 h), P is the average illumination intensity per unit area (70 mW cm⁻²), S is the illuminated area (50 cm²), λ is the selected incident wavelength (480 nm), h is Planck's constant (6.626×10⁻³⁴ J·s), and c is the speed of light (3.0×10⁸ m).

1.9 DFT calculations

Density functional theory (DFT) calculations were performed using the Vienna Ab initio Simulation Package (VASP)⁴. The core electrons were modeled using the projector-augmented-wave (PAW) method and the electron exchange and correlation were described by the generalized gradient approximation (GGA) using Perdew-Burke-Ernzerhof (PBE) functional⁵. The plane-wave cutoff energy was 400 eV. All structures were fully relaxed to their ground state, and spin polarization was considered in all calculations. Geometry optimizations were carried out using the conjugate gradient method, with convergence criteria of set to 10⁻⁵ eV in energy and 0.02 eV/Å in force. The Brillouin zone integration was performed using a Monkhorst-Pack mesh with sizes 3 × 3 × 1 K-point for both structural geometry optimization and subsequent property calculations^{6,7}.

1.10 Interfacial electric field calculation

Both the zeta potential and surface potential of 20 %-Co₂SnO₄@ZnIn₂S₄ are higher than those of pure ZnIn₂S₄, which indicates that the interfacial electric field of 20 %-Co₂SnO₄@ZnIn₂S₄ is higher than that of the pure ZnIn₂S₄ according to the following equation developed by Kanata et al ^{8,9}.

$$F_s = (-2V_s\rho/\varepsilon\varepsilon_0)^{1/2} \quad (1)$$

Where F_s is the magnitude of the internal electric field magnitude, V_s is the surface voltage, ρ is the surface charge density, ε is the low-frequency dielectric constant, and ε_0 is the permittivity of free space. This equation demonstrates that the internal electric field magnitude is primarily determined by the surface voltage and the charge density, as ε and ε_0 are constants. The surface potential V_s is obtained using AFM in surface potential mode, while the ρ is determined by the zeta potential and calculated using the Gouy-Chapman model:

$$\sigma = \sqrt{8kT\varepsilon\varepsilon_0n} \sinh\left(\frac{ze\varepsilon_0\varepsilon\psi_0}{2kT}\right) \quad (2)$$

Among the relevant equations, for smaller Zeta potential values ($\psi_0 < 50\text{mV}$), the surface potential ψ_0 can be expressed as ¹⁰:

$$\psi_0 = \zeta\left(1 + \frac{D}{a_1}\right)e^{\kappa D} \quad (3)$$

σ —surface charge density, C/m²

k —the Boltzmann constant, J/K

T —absolute temperature, K⁻¹

ε —relative medium constant

ε_0 —vacuum dielectric constant, F/m

n —number of electrolytes per unit volume, m⁻³

e_0 —electron charge, C

z —electrolyte valence

ψ_0 —surface potential, V

a_1 —particle Stokes radius, m

ζ —zeta potential

κ^{-1} —Debye length, nm

D—distance from Sliding Layer to Particle Surface

The intensity of the interfacial electric field (IEF) can be calculated according to the following equation:

$$E = [AV_{sp} \sin h(\frac{ze_0\zeta(1 + \frac{D}{a_1})e^{kD}}{2kT})]^{1/2}$$

2. Supplementary Figures and Tables

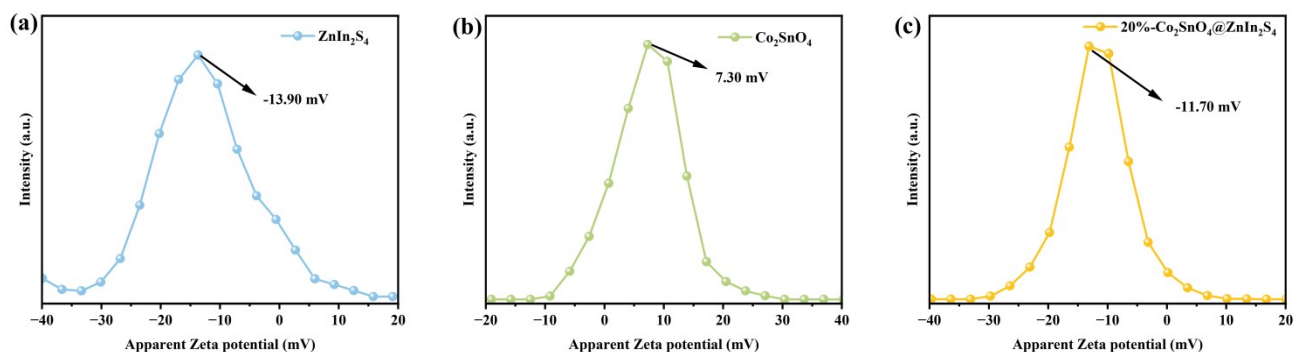


Fig. S1 The zeta potentials of (a) ZnIn₂S₄, (b) Co₂SnO₄, and (c) 20%-Co₂SnO₄@ZnIn₂S₄ dispersed in pure water.

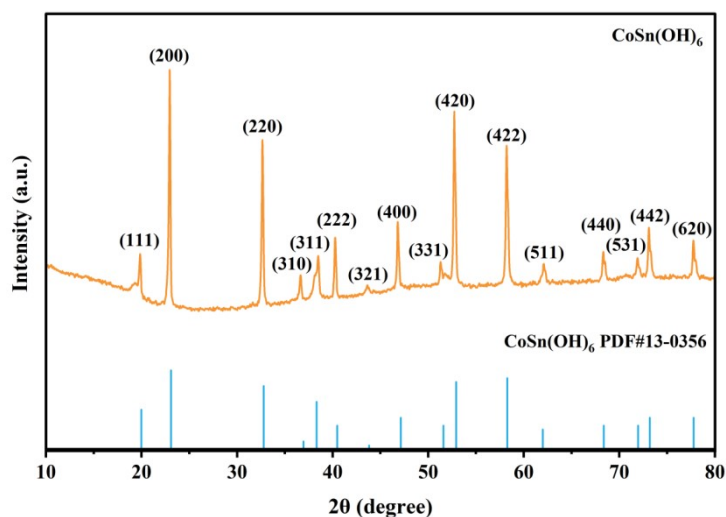


Fig. S2 XRD diffractograms of CoSn(OH)₆.

Note: CoSn(OH)₆ plays a pivotal role in the synthesis of Co₂SnO₄ as it serves as a precursor. CoSn(OH)₆ is initially formed through the reaction of Co(NO₃)₂•6H₂O and SnCl₄•5H₂O in the presence of NaOH, followed by precipitation. This CoSn(OH)₆ is then subjected to high temperature calcination, which facilitates the transformation into Co₂SnO₄ nanoparticles, essential for photocatalytic applications.

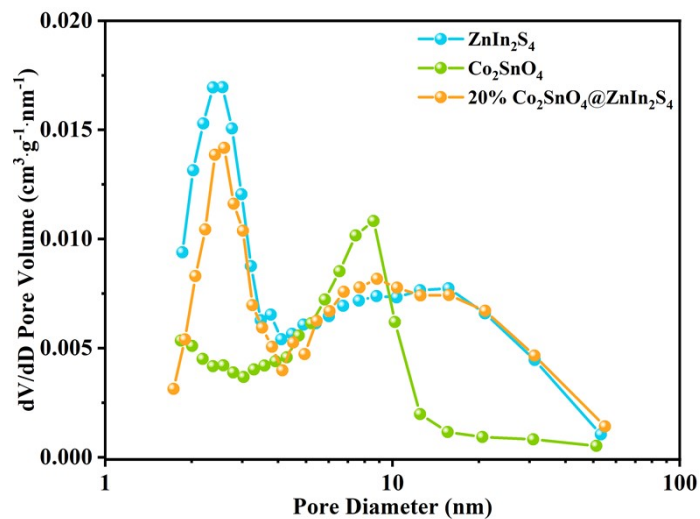


Fig. S3 Pore size distribution curves of Co_2SnO_4 , ZnIn_2S_4 and 20%- $\text{Co}_2\text{SnO}_4@\text{ZnIn}_2\text{S}_4$.

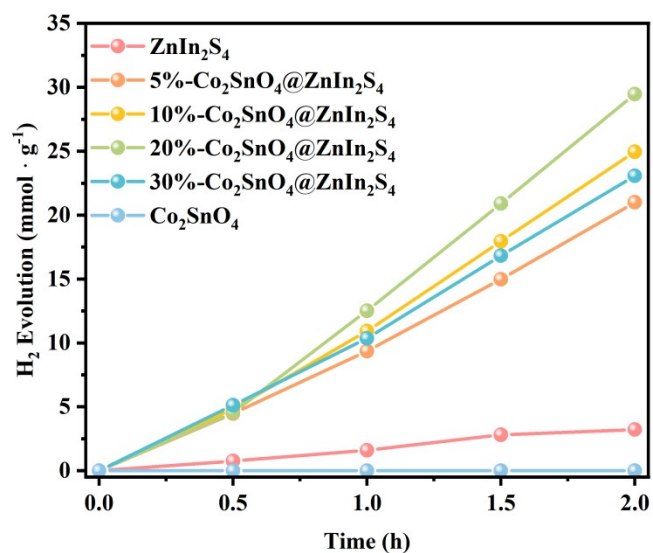


Fig. S4 Temporal evolution of photocatalytic H_2 evolution on Co_2SnO_4 , ZnIn_2S_4 and $x\%-\text{Co}_2\text{SnO}_4@\text{ZnIn}_2\text{S}_4$.

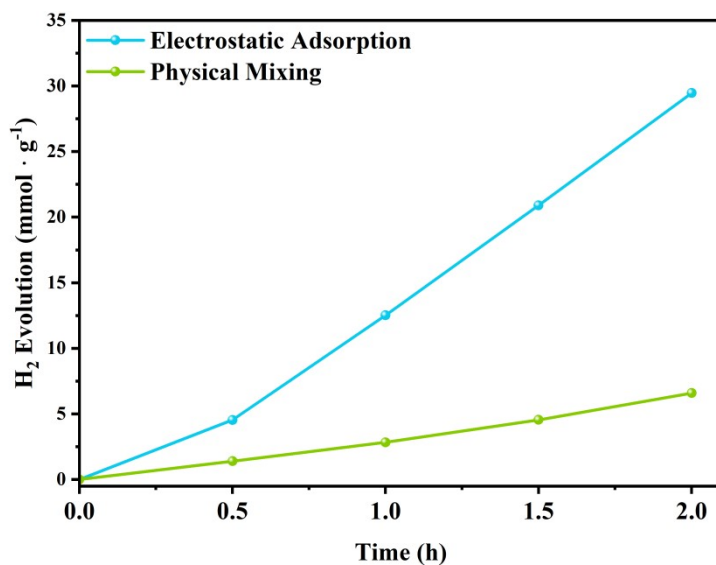


Fig. S5 Time profiles of photocatalytic H₂ evolution of 20 %-Co₂SnO₄@ZnIn₂S₄ for different preparation methods.

Note: Physical mixing is defined as the straightforward combination of Co₂SnO₄ and ZnIn₂S₄ powders, achieving a weight ratio of 20% Co₂SnO₄ to ZnIn₂S₄, utilizing a mortar.

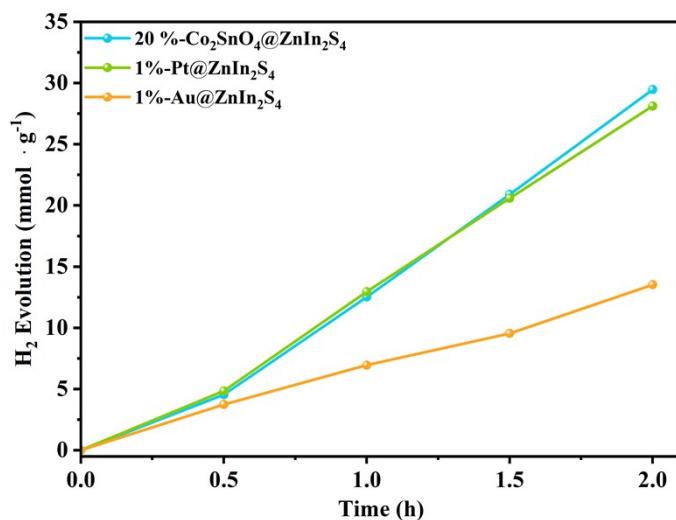


Fig. S6 Time profiles of photocatalytic H₂ evolution of 20 %-Co₂SnO₄@ZnIn₂S₄, 1 %-Pt@ZIS and 1 %-Au@ZIS under Xenon light illumination.

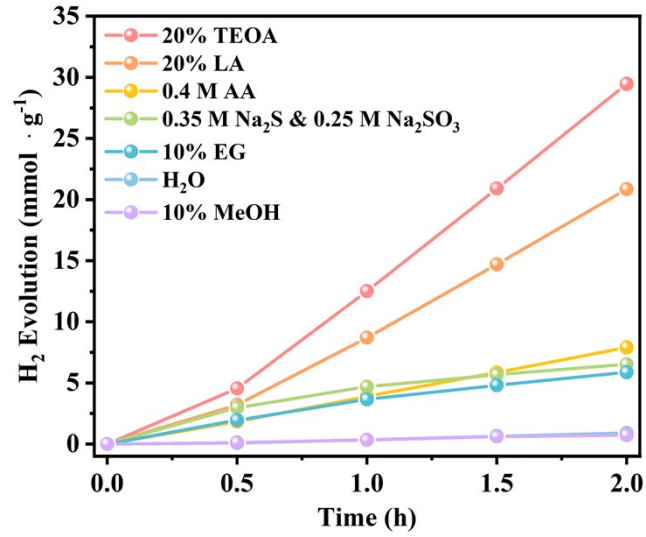


Fig. S7 Time profiles of the calculated H₂ evolution with various sacrifice agents for the 20%-Co₂SnO₄@ZnIn₂S₄ S-scheme heterojunction.

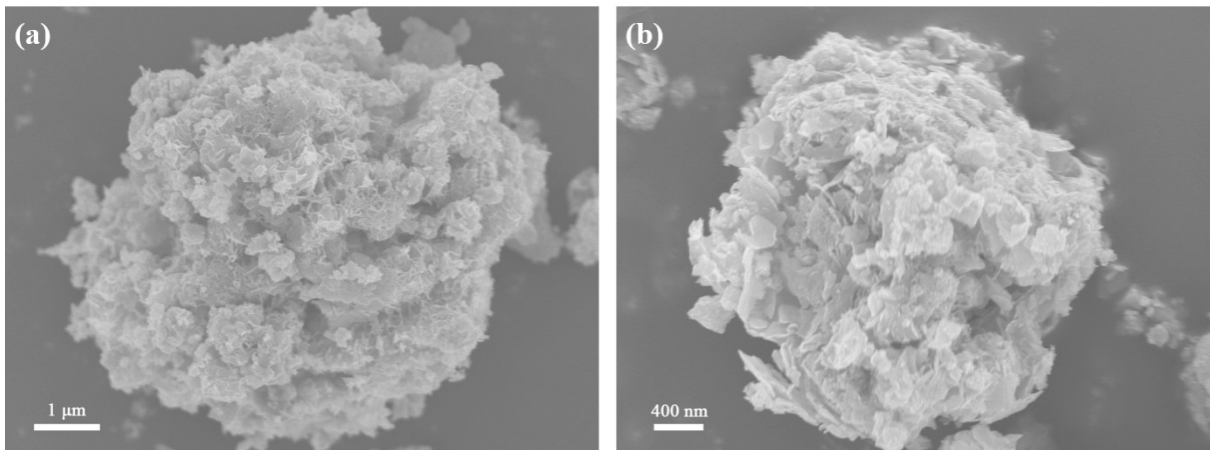


Fig. S8 SEM images of the (a) fresh and (b) used 20%-Co₂SnO₄@ZnIn₂S₄.

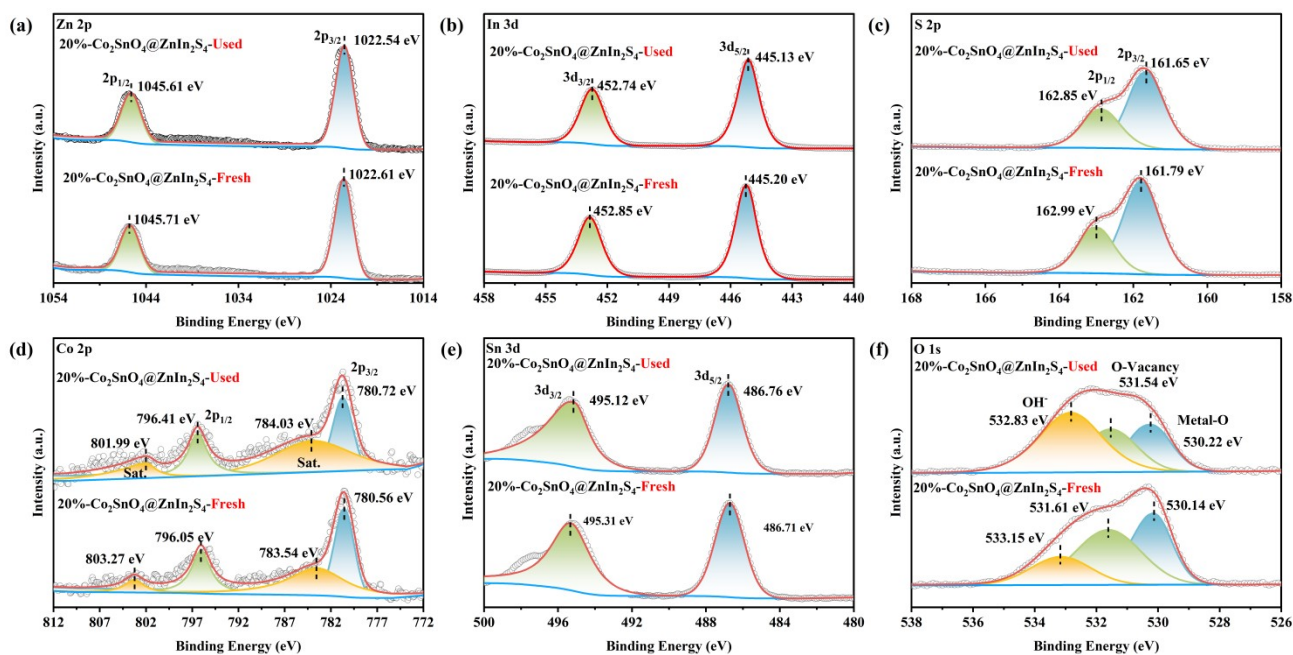


Fig. S9 High-resolution XPS spectra of the fresh and used 20%-Co₂SnO₄@ZnIn₂S₄: (a) Zn 2p, (b) In 3d, (c) S 2p, (d) Co 2p, (e) Sn 3d, and (f) O 1s.

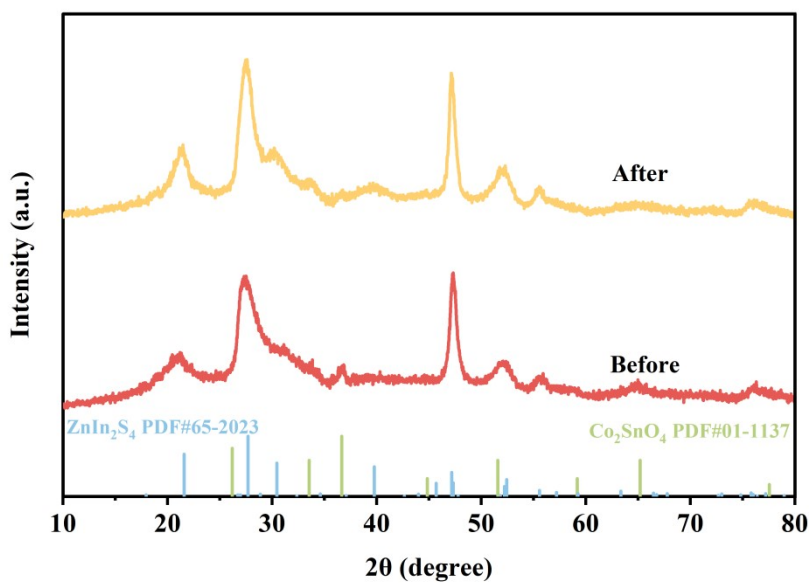


Fig. S10 XRD patterns of 20%-Co₂SnO₄@ZnIn₂S₄ before and after reaction.

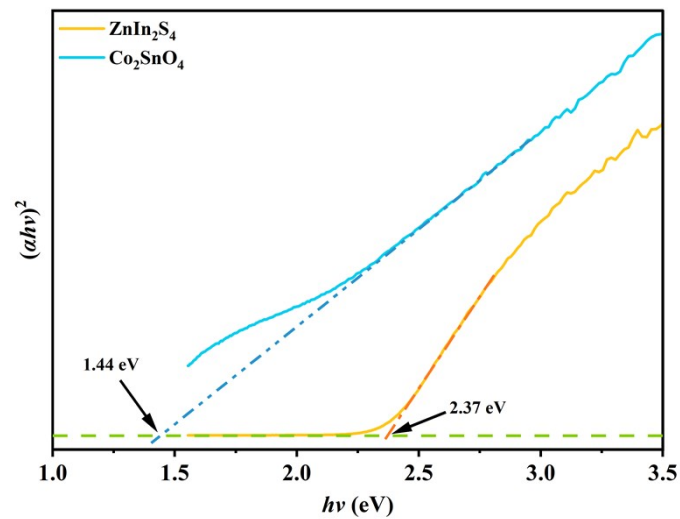


Fig. S11 Tauc plots of Co₂SnO₄ and ZnIn₂S₄.

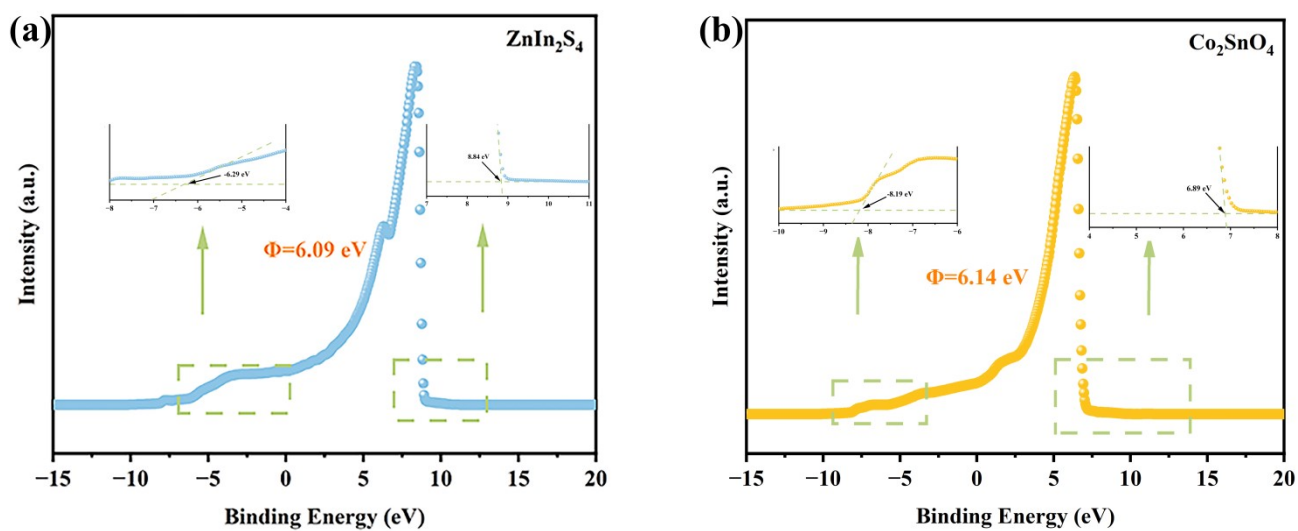


Fig. S12 UPS spectra of (a) ZnIn₂S₄ and (b) Co₂SnO₄.

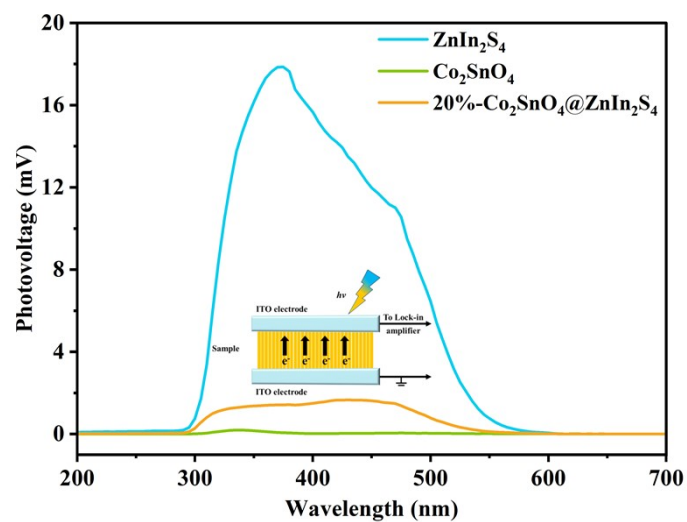


Fig. S13 SPV of ZnIn_2S_4 , Co_2SnO_4 and $20\%-\text{Co}_2\text{SnO}_4@\text{ZnIn}_2\text{S}_4$.

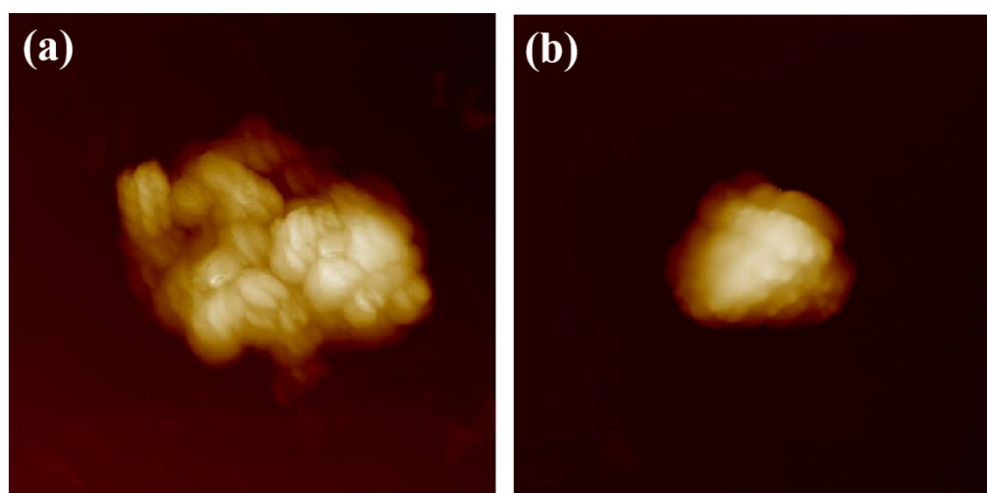


Fig. S14 AFM images of (a) ZnIn_2S_4 and (b) $20\%-\text{Co}_2\text{SnO}_4@\text{ZnIn}_2\text{S}_4$.

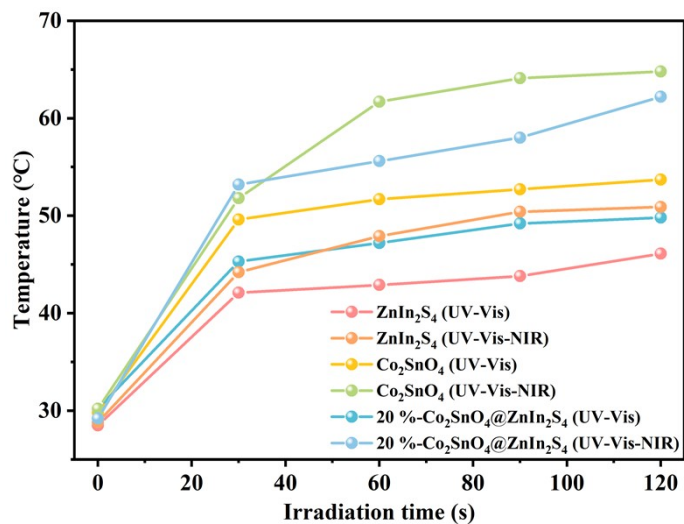


Fig. S15 Temperature variation curve of ZnIn₂S₄, Co₂SnO₄ and 20%-Co₂SnO₄@ZnIn₂S₄ under UV-vis and UV-vis-NIR illumination.

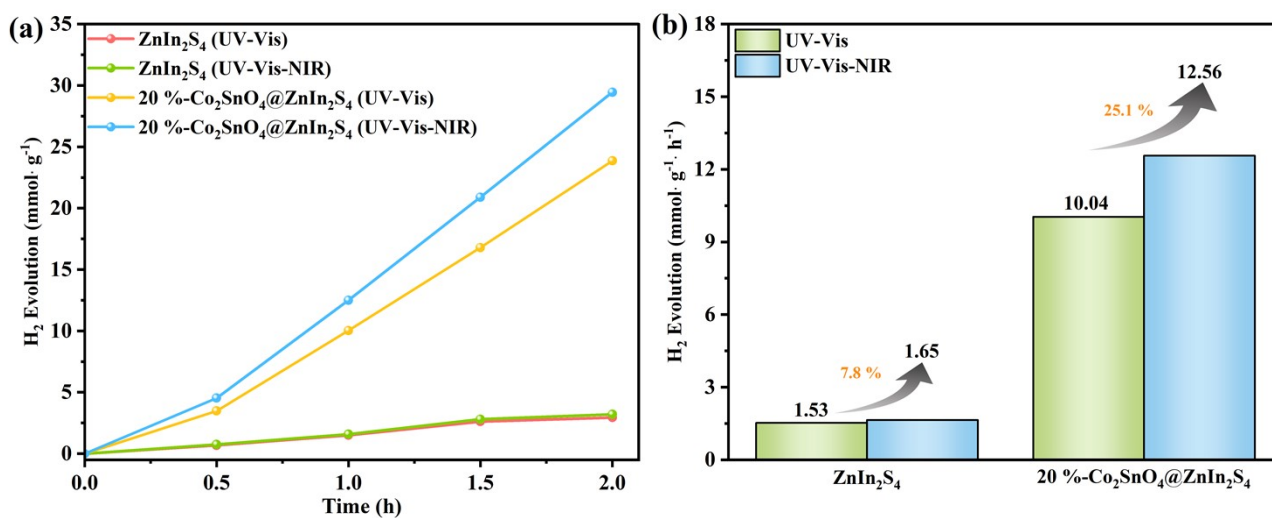


Fig. S16 Time profile (a) and the corresponding H₂ evolution rate (b) of ZnIn₂S₄ and 20%-Co₂SnO₄@ZnIn₂S₄ under the different light illumination.

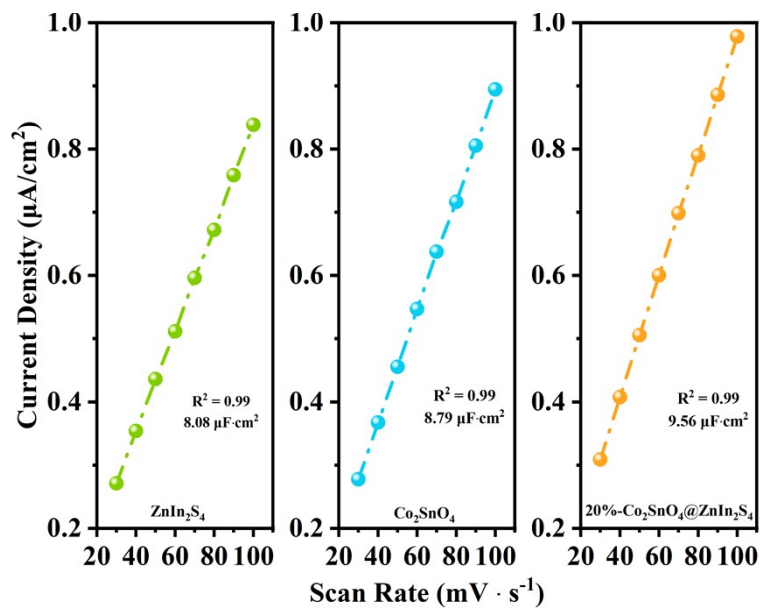


Fig. S17 The linear fitting curve of capacitance current and scanning rate obtained from Figs. 7d-f.

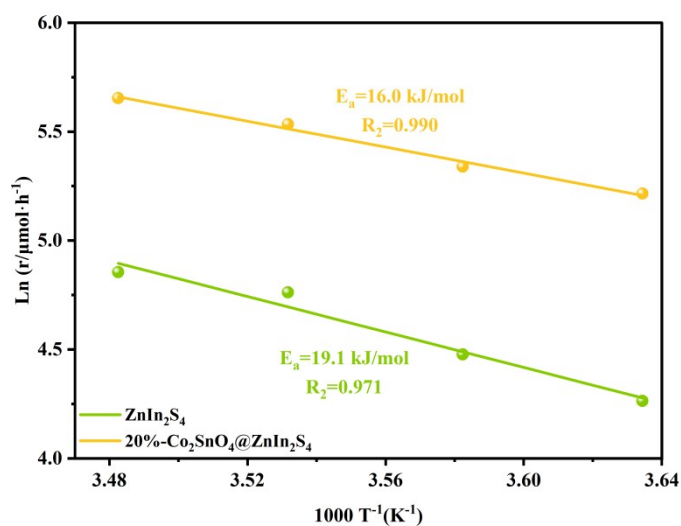


Fig. S18 Temperature dependence of the H_2 evolution rate and corresponding comparison of apparent activation energy of ZnIn_2S_4 and 20%- Co_2SnO_4 @ ZnIn_2S_4 .

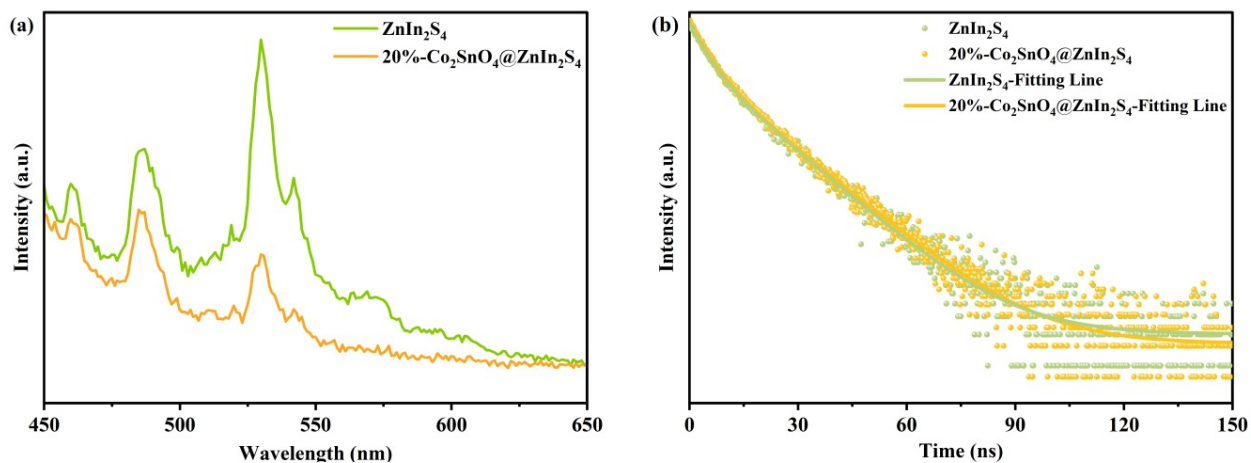


Fig. S19 (a) Steady-state and (b) transient PL spectra of ZnIn₂S₄ and 20%-Co₂SnO₄@ZnIn₂S₄.

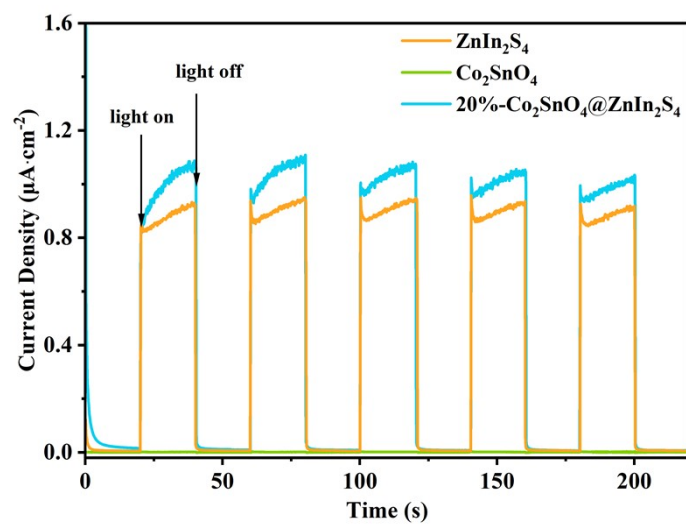


Fig. 20 Transient photocurrent response curves of Co₂SnO₄, ZnIn₂S₄ and 20%-Co₂SnO₄@ZnIn₂S₄.

Table S1. BET specific surface area (S_{BET}), pore volume (V_{pore}) and pore diameter (D_{pore}) of the as-prepared samples.

Sample	S_{BET} ($\text{m}^2 \text{g}^{-1}$)	V_{pore} ($\text{cm}^3 \text{g}^{-1}$)	D_{pore} (nm)
ZnIn ₂ S ₄	102.36	0.462	15.71
20 %- Co ₂ SnO ₄ @ZnIn ₂ S ₄	94.59	0.443	16.46
Co ₂ SnO ₄	46.84	0.220	14.17

Table S2. Comparison of H₂ evolution using different materials.

Main photocatalyst	Light source	Sacrificial agent	Hydrogen production rate	Reaction temperature	Ref.
Co ₂ SnO ₄ @ZnIn ₂ S ₄	300 W Xenon lamp	TEOA (20 %)	12.56 mmol g ⁻¹ h ⁻¹	6 °C	This work
Co ₃ O ₄ @ZnIn ₂ S ₄	300 W Xenon lamp ($\lambda > 420$ nm)	TEOA (20 %)	4.52 mmol g ⁻¹ h ⁻¹	6 °C	11
Carbon@ZnIn ₂ S ₄	300 W Xenon lamp	TEOA (10 %)	2.97 mmol g ⁻¹ h ⁻¹	12 °C	12
CDs/Ni ₃ P/ZnIn ₂ S ₄	300 W Xenon lamp		1.88 mmol g ⁻¹ h ⁻¹	50 °C	13
NiCo ₂ S ₄ /ZnIn ₂ S ₄	300 W Xenon lamp ($\lambda > 420$ nm)	TEOA (10 %)	10.29 mmol g ⁻¹ h ⁻¹	5 °C	14
FeSe ₂ @ZnIn ₂ S ₄	300 W Xenon lamp ($\lambda > 400$ nm)	0.25 M Na ₂ SO ₃ & 0.35 M Na ₂ S	7.64 mmol g ⁻¹ h ⁻¹	5 °C	15

Table S3. EIS data for the ZnIn₂S₄, 20%-Co₂SnO₄@ZnIn₂S₄ and Co₂SnO₄

Photocatalyst	R _s (Ω)	R _{ct} (kΩ)	CPE-T	CPE-P
ZnIn ₂ S ₄	38.93	1.132 × 10 ⁴	1.366 × 10 ⁻⁵	0.9679
20 %-Co ₂ SnO ₄ @ZnIn ₂ S ₄	37.27	6.056 × 10 ³	1.381 × 10 ⁻⁵	0.9665
Co ₂ SnO ₄	35.06	1.706 × 10 ⁴	1.465 × 10 ⁻⁵	0.9717

Table S4. Fluorescence lifetimes of the ZnIn₂S₄ and 20%-Co₂SnO₄@ZnIn₂S₄

Sample	τ ₁ (ns)	A ₁	τ ₂ (ns)	A ₂	τ _A (ns)
ZnIn ₂ S ₄	4.21	7.323	14.40	0.928	7.29
20 %- Co ₂ SnO ₄ @ZnIn ₂ S ₄	4.71	6.099	15.15	0.845	8.09

References

1. Q. Yu, S. Sun, A. R. Puente-Santiago, C. Wu, X. Xiong, Y. Jin and B. Weng, *Appl. Catal. B Environ*, 2025, **367**, 1259098
2. X. Guo, Q. Xiao, T. Yang, Y. Liu and Z. Jin, *Sep. Purif. Technol*, 2023, **325**, 124764.
3. T. Morikawa, S. Sato, K. Sekizawa, T. Arai and T. M. Suzuki, *Chemsuschem*, 2019, **12**, 1807-1824.
4. G. Kresse and J. Furthmüller, *Comput. Mater. Sci*, 1996, **6**, 15-50.
5. Perdew, Burke and Ernzerhof, *Phys. Rev. Lett*, 1996, **77**, 3865-3868.
6. S. Grimme, S. Ehrlich and L. Goerigk, *J. Comput. Chem*, 2011, **32**, 1456-1465.
7. S. Grimme, J. Antony, S. Ehrlich and H. Krieg, *J. Chem. Phys*, 2010, **132**, 154104-154104.
8. J. Li, G. Zhan, Y. Yu and L. Zhang, *Nat. Commun*, 2016, **7**, 11480.
9. J. Li, L. Cai, J. Shang, Y. Yu and L. Zhang, *Adv. Mater*, 2016, **28**, 4059-4064.
10. C. Liu, Y. Zhang, J. Wu, H. Dai, C. Ma, Q. Zhang and Z. Zou, *J. Mater. Sci. Technol*, 2022, **114**, 81-89.
11. S. Zhang, G. Zhang, S. Wu, Z. Guan, Q. Li and J. Yang, *J. Colloid Interface Sci*, 2023, **650**, 1974-1982.
12. P. Shan, K. Geng, Y. Shen, P. Hao, S. Zhang, J. Hou, J. Lu, F. Guo, C. Li and W. Shi, *J. Colloid Interface Sci*, 2025, **677**, 1098-1107.
13. J. Jia, X. Guo, Y. Tang, W. Zeng, H. Zeng and Z. Rui, *Int. J. Hydr. Energy*, 2025, **104**, 122-130.
14. Y. Guo, L. Mao, Y. Tang, Q. Shang, X. Cai, J. Zhang, H. Hu, X. Tan, L. Liu, H. Wang, T. Yu and J. Ye, *Nano Energy*, 2022, **95**, 107028.
15. X. Liu, S. Wang, J. Cao, J. Yu, J. Dong, Y. Zhao, F. Zhao, D. Zhang and X. Pu, *J. Colloid Interface Sci*, 2024, **673**, 463-474.